A thermal energy harvester using LaFeSi magnetocaloric materials

Smail Ahmim, Morgan Almanza, Vincent Loyau, Alexandre Pasko, Frédéric Mazaleyrat, Martino Lobue

A thermal energy harvester using LaFeSi magnetocaloric materials

Smail Ahmim[1], Morgan Almanza[1], Vincent Loyau[1], Alexandre Pasko[1], Frédéric Mazaleyrat[1], and Martino LoBue[1]
[1]SATIE, ENS Paris-Saclay, CNRS, Université Paris-Saclay, 91190 Gif-sur-Yvette, France

A thermomagnetic generator (TMG) using an Halbach structure as a field source and a first order LaFeSi magnetocaloric material (MCM) from Vacuumschmelze as active substance, is presented. The MCM, suspended on a cantilever beam self oscillates between a hot source and a heat sink. The mechanical energy associated with the oscillation is harvested and converted into electricity using piezoelectric materials. This system is working between a 18°C cold end, and a 56 °C heat source (i.e. over a temperature difference between reservoirs $\Delta T_{res} = 38$ °C) and shows a power of 0.12μW (6.8 μW per 1 cm^3 of MCM). We present and discuss a detailed analysis of the thermodynamic cycle underpinning the device mechanism, relying on direct measurements on the working prototype and on a full laboratory characterization of the MCM. Although our system shows a state-of-the-art power output, our analysis gives useful clues towards further performance improvements.

***Index Terms*—thermal engine, magnetocaloric materials, pyromagnetic effect, energy harvesting, thermodynamics**

I. Introduction

The development of efficient and high throughput energy recovery devices represents a growing area of research aiming the improvement of global energy efficiency on the one hand, and the design of generators to power-up the new generation of Internet of Things (IoT) small autonomous devices on the other. Besides an increased battery life due to improved efficiency and full autonomy are closely entwined objectives.

Thermoelectric devices offer a direct conversion path from a heat flux to electricity; however their low factor of merit, and heat leakages critically reduce their reliability particularly when working on small temperature differences, and on length scales of few millimeters [1].

Nowadays, about two decades since the discovery of giant magnetocaloric effect [2] we have an unprecedented choice between many families of magnetocaloric materials (MCM) that have been mostly optimized to be used in room temperature magnetic cooling devices [3]. This state of affairs gives us an unique opportunity to revisit the TMG concept dating from Tesla and Edison patents (see [4] and references therein) and to bring it towards a real technological breakthrough.

Modifying the magnetic order (e.g. ferromagnetic to paramagnetic or vice-versa) through a temperature change is the core of TMG functioning. The conversion to electrical energy is either done directly via Faraday's law or through an intermediate step into mechanical energy which is eventually converted by a transducer. Waste heat harvesting often imply an imposed temperature difference ΔT_{res} between the hot source and the heat sink, so that the power output as a function of ΔT_{res} is commonly used as a figure of merit. Some promising results have been obtained at $\Delta T_{res} \approx 100$ °C. Recently a TMG showing an average electrical power density of 118 mWcm^{-3} for $\Delta T_{res} = 140$ °C has been reported [1]. Working on a slightly smaller temperature difference (i.e. $\Delta T_{res} = 80$ °C) another group assembled a 38 mW/cm^3 TMG [5].

However most of the waste heat available reservoirs are in the so called *low grade* form, with a ΔT_{res} of a few tens degrees, and this explains the focus of many studies on smaller temperature spans. Indeed more than ten years since an output power of 28.34 mW/cm^3 has been estimated [6] for a device using piezoelectric transducers and working on $\Delta T_{res} = 50$ °C. More recently a TMG showing a power density of 1.6 μW/cm^3, and working on $\Delta T_{res} \approx 25$ °C has been presented [7], while up to 0.32 mW/cm^3 have been reported [8] from a Faraday's law based device [8] working on $\Delta T_{res} = 30$ °C.

The perspective to convert heat directly into electricity through Faraday's law is extremely attractive and, beside the outstanding results from [8], allows to avoid some of the difficulties associated with an additional conversion step (heat to mechanical, and mechanical to electric). Nevertheless a major shortcoming of this approach comes from the fluid based thermal exchange mechanism it generally relies on. Indeed the use of an energy consuming pump acting on the liquid heat exchanger drastically reduces the overall power output and gives-up device autonomy, an even more detrimental issue for IoT, biomedical [9], and embedded applications [10]. Instead the mechanical energy intermediate step allows to collapse into the very same process (viz. the movement of the active caloric material between the hot and the cold end) the caloric effect and the thermal switch, making possible a compact integrated system where the active substance is also the pump [11].

The mechanical energy stage has been used jointly with micro-coil based Faraday's law pick-up to enhance the device power output [1], while some authors relied on an electroactive material as a final transducer [5]. The use of piezoelectric materials has been proposed by many authors [6], [12]. The main advantages of this approach are the relative simplicity of integration and the good transduction efficiency even at low working frequencies.

The design proposed here is similar to the one presented in [6] with the following differences: the active substance undergoes a first order magnetic transition (i.e. a commercial La(FeSi)$_{13}$H from Vacuumschmelze [13], [14]) instead of a continuous one (e.g. a Gd plate in [6]); the magnetic field source has been optimized in order to achieve higher field, and to minimize the demagnetizing field (i.e. Halbach structure); piezoelectric transducers have been integrated in the device.

Moreover the position of the moving cantilever are measured while the device is working jointly with the power output allowing to extrapolate the actual thermodynamic cycle undergone by the active material. Our prototype shows a 0.12μW power-output with a density of 6.8 μWcm^{-3} per volume of MCM. In what follows we shall discuss these results and the main differences we measured between the experimentally determined working cycle and the ideal Brayton cycle the original design was aiming at.

II. Thermomagnetic generator

In our TMG (Fig. 1) a La(FeSi)$_{13}$H plate from Vacuumschmelze has been used as active material. The plate is suspended on a cantilever. When the MCM is ferromagnetic, the magnetic force is predominant and the MCM moves towards the field source situated on the hot reservoir. When the material is paramagnetic, the cantilever recoil force brings it back to the heat sink. During the contact with the hot and cold ends the MCM passes respectively from ferromagnetic to paramagnetic state and vice-versa. The device has been designed in order to self-oscillate and to work on a magnetic Brayton cycle.

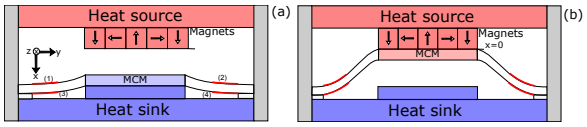

Figure 1. A schematic representation of our piezoelectric based thermomagnetic generator : a) the MCM is in direct contact with the heat sink, b) the MCM is in contact with the hot source and with the Halbach array. Piezoelectric plates glued on the cantilever beam are represented as thicker lines (red in online version).

The proposed device (Fig. 2) has been designed and assembled in order to directly measure most of the relevant variables describing the working TMG cycle. The MCM is a (La(Fe,Si)$_{13}$H) plate ($0.25 \times 7 \times 10$ mm^3) with a Curie temperature of $T_C = 30$ °C. The cantilever is a $0.3 \times 20 \times 68$ mm^3 CuBe$_2$ beam. Its stiffness has been measured and is 3266 N m^{-1}. The field source is an Halbach array, built using five NdFeB ($1.5 \times 1.5 \times 10$ mm^3) parallelepiped magnets. This configuration has been chosen to get a high well confined field [15]. The heat source is a heating electrical resistance while the cold reservoir is made with a water exchanger. Both are separated using plastic spacers. The temperature of the heat source and the heat sink are respectively 56 °C and 18 °C ($\Delta T_{res} = 38$ °C).

Four piezoelectric plates (C151 'Soft-PZT' from PI, $0.3 \times 10 \times 10$ mm^3) are glued on the cantilever. Figure 3 shows the measured voltages on each piezoelectric. The average electrical power output of the device is 0.12μW (6.78μ W/cm^3 per volume of the MCM) with a frequency of 0.12 Hz which corresponds to an electrical energy of 1 μJ per cycle.

The displacement of the MCM in Fig. 4 has been measured using a laser sensor (ILD1320 MICRO-EPSILON).

An attempt to measure the temperature of the 250 μm thick material with a 0.2 mm thermocouple gave unreliable results due to thermal inertia of the system.

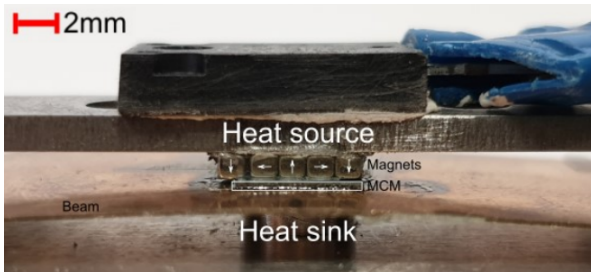

Figure 2. A picture of the device, the heat source on the top with the Halbach array, the white arrows highlight the direction of magnetization of the magnets, the MCM highlighted with white border is bounded on the cantilever beam, the heat sink is the surface on the bottom.

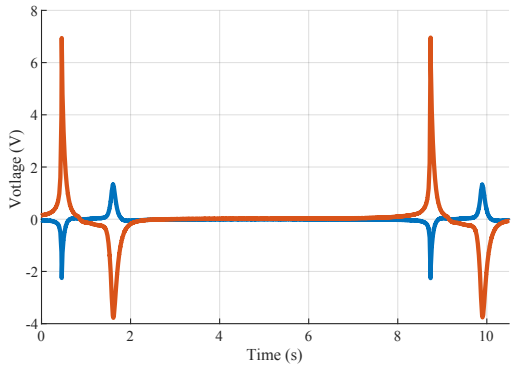

Figure 3. The voltage produced by the piezoelectric plates on the top (red line) and on the bottom of the beam (bottom line).

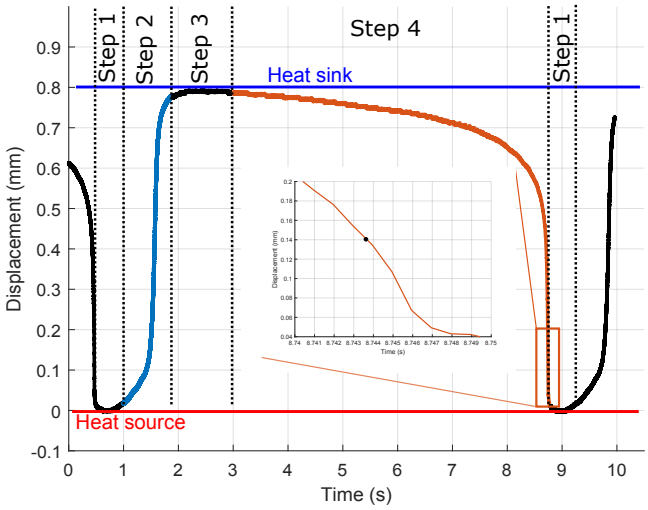

Figure 4. The measured displacement of the MCM. The inset shows an inflection point at 0.14mm during the step 4. The heat source is at 0 mm and the heat sink at 0.8 mm.

III. Working thermodynamic cycle

The device works over a four strokes cycle:

Step 1: When the MCM is in contact with the heat source (Fig. 1 b) the temperature increase drives the phase transition from the ferromagnetic state to the paramagnetic one, resulting in a drop of the magnetic force. At the same time the magnetization reduction decreases the demagnetizing field

increasing the internal field. We estimated the internal field through 3D finite element calculations (Ansys MAXWELL); from the magnetization of the MCM $M(H,T)$, we got the internal field (Fig. 5 line 1). While the applied field remains constant, $\mu_0 H_a = 0.65$ T (rigth dotted line in Fig. 5) , the internal field increases from $\mu_0 H_i = 0.33$ T to $\mu_0 H_i = 0.53$ T.

Step 2: At $T = 55$ °C (point A in Fig. 6), the recoil force of the cantilever becomes larger than the magnetic force. The mechanical instability pushes the MCM back to the heat sink, removing most of the field applied. Along this transformation the adiabatic temperature change is rather small $\Delta T_{adia} \approx 0.1$ °C as apparent in Fig. 5 where the thick black line 2 depicting it mingles with the dashed isotherm. During the displacement the piezoelectric patches deformation produces charges and voltage (Fig. 3).

Step 3: When the MCM is in contact with the heat sink (see Fig. 1 a), it cools-down driving the phase transition from paramagnetic to ferromagnetic. As in step 1, the internal field is calculated using finite element method (Fig. 5 line 3). The increase of the magnetization gradually restores the magnetic force.

Step 4: At 20 °C (point B in Fig. 6), the magnetic force becomes predominant and the mechanical instability drives the MCM back to the heat source. Along the displacement the magnetic field increases. The temperature change during the adiabatic process being $\Delta T_{adia} = 0.2$ °C (Fig. 5 line 4), the process is again nearly isotherm. During the displacement the piezoelectric produces charges and voltage (Fig. 3).

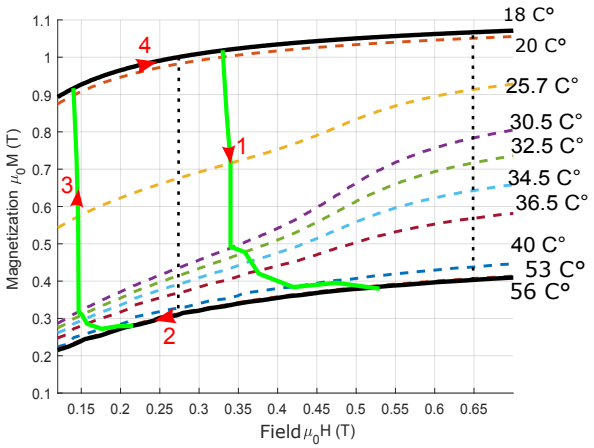

Figure 5. dashed lines: measured isothermal magnetization curves (temperature in the legend). Continuous thick lines: the working cycle taking into account the average internal field. $\Delta T_{adia} = 0.2$ °C and 0.1 °C during steps 2 and 4 respectively. The dotted vertical lines represent the applied fields during the steps 1 (right one at 0.65T) and 3 (left one at 0.27T)

The MCM never reaches the temperature of the reservoirs because the mechanical switching is driven by the temperature of the sample through the magnetic force before complete thermalization is achieved. The competition between the magnetic force and the recoil force of the cantilever produces a mechanical instability stopped by the impact with the hot and the cold ends respectively. This instability drives the MCM towards one side or the other due to the change of total force associated with temperature dependence of the magnetic force. The two temperatures of switching depend on the magnetic field source, on the MCM magnetization, and on the cantilever elastic response. Due to the mentioned difficulties in measuring the MCM temperature we extrapolated the switching temperatures from the measurement of the recoil force and from the computation of the magnetic force (Ansys MAXWELL). The energy per cycle (viz. the area of the mechanical cycle shown in Fig. 6) calculated from our numerical simulations, using the LaFeSi data, is $E_{num} = 3.5$ mJ. As the total energy per cycle picked-up by the piezoelectric transducers is $E_{piezo} = 1$ μJ, namely three order of magnitudes lesser than what could be harvested, a detailed analysis of the real cycle is necessary in order to define an appropriate optimization strategy. This analysis has been done by extrapolating the actual working cycle from the displacement measurements: indeed Newton's second law can be used to calculate the total force F_{tot} (i.e. the resultant of all the relevant forces) acting on the system MCM-beam. The acceleration of the MCM is obtained from the time second-derivative of the measured displacement shown in Fig. 4. Knowing the deformation of the cantilever from finite element simulation according to the displacement of the MCM, we deduce the kinetic energy associated to each element of the cantilever. The deformation depending linearly on the displacement, we work-out the equivalent mass of the overall system. The equivalent mass is found to be $m_e = m_{MCM} + \frac{1}{2.5} m_b$ (where m_{MCM} and m_b are the masses of the material and of the beam respectively). Fig. 7 shows the speeds as a function of the displacement during step 2 (dashed blue line) and 4 (continuous red line), Fig. 8 shows the total force acting on the MCM-beam system as a function of the displacement. It is worth noting that F_{tot} has been extrapolated from direct displacement measurements. In our ideal cycle as described above and as represented in Fig. 6, there are only three relevant forces, the magnetic force F_{mag} along transformation 2 and 4 (lower dashed blue line, and upper red continuous line respectively), the beam recoil force F_r (straight green line between A and B) and the force associated with the piezoelectric deformation F_{piezo} which is too small to be represented in Fig. 6 (i.e. it is indistinguishable from F_r at the chosen scale). Neglecting the piezoelectric force, the total force is $F_{tot} \approx F_{mag} - F_r$ so that F_{tot} is expected to lay between zero (point A and B where $F_{mag} = F_r$) and about 10 N along step 4, and of the order of 1 N in step 2. From Fig. 8 it is apparent that the actual force acting on the beam is much lower, namely in the range of 10^{-3} N along step 4, and of 10^{-5} N in step 2, as a consequence the cycle area gets reduced down to 139μJ. Piezoelectric picking only 1 μJ, we are still far from our numerical simulations $E_{num} = 3.5$ mJ. Notwithstanding the sub-optimal piezoelectric conversion efficiency, our foremost concern is the dramatic difference between the theoretical forces and the ones deduced from experiment.

IV. Discussion and Conclusions

The electrical output we report matches the state of the art for low grade heat TMG harvesters (see table I), nonetheless

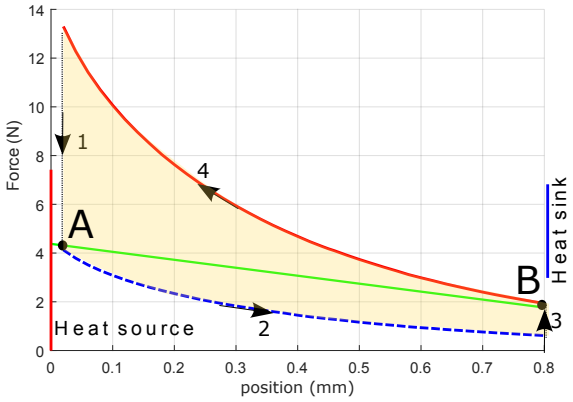

Figure 6. The theoretical cycle, filled area between the simulated magnetic forces (using a 3D finite element model) at 20 and 55°C (upper red curve (4) and lower blue dashed curve (2)). The cantilever recall force is represented by the green line. The four steps are represented all along the cycle. The heat source is at the origin (0 mm) and the heat sink is at 0.8mm. A and B are the points where the cantilever moves away from the contact with the reservoirs.

the difference between the simulated cycle and the actual one hints at the opportunity of further improvements of our device.

The main issue here is clearly related to the fact that we experience a drastically reduced magnetic force with respect to the one our calculations predicted. Another, somewhat related issue is the asymmetry of the cycle, apparent in Fig. 4 where step 2 lasts about 1 second, while step 4 is about six times longer.

Let us now examine in detail step 4 using , Fig. 4, 7, and 8. The displacement can be split into four distinct sections as done in Fig. 8.

(I) From 0.8 and 0.5 mm displacement, we see in Fig. 4 that the MCM nearly immediately lose the direct contact with the heat sink; during this phase the material exchanges heat through air making the cooling and the phase transition progress slower than predicted. (II) From 0.5 to 0.2 mm displacement we can appreciate from Fig. 8 an increase in F_{tot} that can be related to the transition progress and to the consequent growth in the ferromagnetic volume fraction, as well as to the increasing field gradient associated with the slight position change. (III) From 0.2 to 0.14 mm displacement F_{tot} increases steeply until reaching its maximum of $\approx 6 \times 10^{-3}$N corresponding to the inflection point shown in the Fig. 4) inset, this force is four orders of magnitude lower than the theoretical expectation (i.e. ≈ 10 N). (IV) Eventually, from 0.14 mm to the contact with the heat source the force decreases and becomes negative (point b_1 in Fig. 8), something that can hardly be explained without introducing an additional force beside the beam recoil and the magnetic ones.

This behavior can be explained as follows. (I) The first part relates to an improper tuning of the magnetic and the recoil force causing the loss of thermal contact and a consequent reduction of the device working frequency; this is a problem related to the difficulty to actually ensure, through a fine control of the design, an unstable equilibrium point in B, namely a tangent of the magnetic force in B Fig. 6 steeper than the slope of the beam force. Point B has been designed in order to get close to a bifurcation point. Unfortunately fabrication uncertainty has led the dynamical system trajectory through a family of mechanical stable points. Fortunately those points are close enough to the heat sink to keep the heat transfer. Even if the transfer is reduced, slowing down the cycle, it eventually drives the system to an instability essential to trigger the second part of the step 4. (II) The MCM-beam system strongly accelerates, the field decrease and most of the phase transition takes place. The MCM moving faster and faster towards the field source, we can assume that the air squeezing between the moving MCM and the hot reservoir results in an improvement of the convective heat transfer. This air in this gap being hot, it prematurely rises the LaFeSi plate temperature causing a magnetization and magnetic force dramatically lower than expected. (III) When the gap is too thin, viscous reaction of the air and/or eddy currents in the MCM cause an additional dissipative force at the origin of F_{tot} reversal in the last section of the displacement (point b_1 in Fig. 7 and 8). (IV) Eventually, the material stops in contact with the hot end. A rather similar analysis can be done on the displacement along the step 2 (dashed blue lines in Fig. 7 and 8).

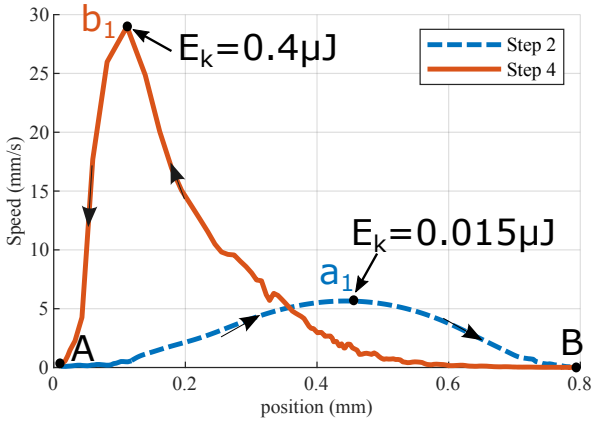

Figure 7. The speed of the MCM vs its displacement. The speed is computed by differentiating the measured displacement by time. E_k is the kinetic energy associated with the two speed maxima.

Taking into account the heat transfer is essential to pass from a quasi-static analysis of the theoretical cycle to a finite time analysis [16]. The working cycle we presented here shows a non-negligible switching time (more than 90% of the period indeed) as well as departures from adiabaticity. These issues will have to be addressed when modeling our device in the frame of a finite time thermodynamics approach [17], a development we shall study elsewhere.

A first and relatively easy improvement of our device will come from increasing the piezoelectric based energy transduction. Here the advantage will be two-fold as we shall harvest an higher fraction of the available energy on the one hand, and on the other reduce the air squeezing by slowing down the MCM speed.

More importantly a wiser control of the magnetic versus recoil force balance, and a better thermal management will allow to modify the thermodynamic cycle getting closer to the theoretical one, a cycle somewhat in between a Brayton and an Ericsson one. This objective will be possible only through a

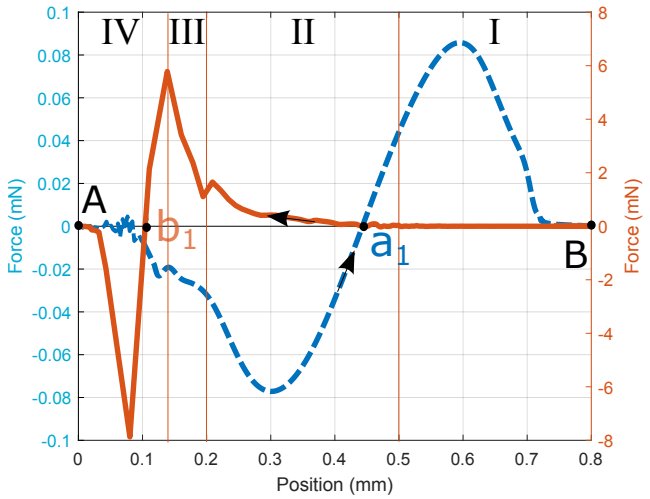

Figure 8. The total force F_{tot} acting on the moving part, extrapolated from its effective mass and the measured displacement, as a function of the displacement for step 2 (dashed blue line, scale on the left), and for step 4 (continuous red line, scale on the right). Sections I, II, III, IV refer to the red curve (step 4) and are described in the main text.

Table I
COMPARISON WITH DIFFERENT TMG PROTOTYPES

	Electrical power	ΔT_{res}	Transducers	Comments
This Work	6.8 μW/cm^3	38 °C	Piezoelectric materials	measured results
[7]	1.6 μW/cm^3	25 °C	Coils	measured results
[6]	28.34 mW/cm^3	50 °C		the power is estimated
[8]	0.32 mW/cm^3	30 °C	Coils	Maximum Power, no information on the input power
[1]	118 mW/cm^3	140 °C	Coils	measured results
[5]	38 mW/cm^3	80 °C	PVDF	measured results

better screening of the state variables, notably of the material temperature that, due to the mentioned problems, has not been directly measured in the present set-up.

We presented a millimeter scale TMG with an Halbach structure as a field source, and a commercial LaFeSi plate as active material, harvesting 1 μJ energy per cycle working over a temperature difference between reservoirs $\Delta T_{res} = 38$ °C. Simulations considering the magnetic field source and the material properties emphasizes the changes in the internal field due to the demagnetizing factor and its known [18] effect on the adiabatic temperature change. The main shortcomings of the present set-up, limiting its energy per cycle and its frequency (i.e. its power output) have been identified and discussed. On the one hand improving the electro-mechanical energy conversion efficiency, and tackling the detrimental effect of the air squeezing in the gap between the reservoirs will allow an increase of the energy output per cycle. On the other, optimization of the self-oscillating dynamics with a better interplay between the force balance and the thermal exchange time will pave the way to a relevant frequency increase. Nevertheless the electric power we get (0.12 μW or 6.8$\mu W/cm^3$) is comparable with similar results obtained from reported TMG prototypes working on comparable low grade heat sources as shown in table I.

ACKNOWLEDGMENT

This work benefited from the financial support of the project HiPerTherMag (ANR-18-CE05-0019) managed by the French National Research Agency. We would like to thank Dr. Alex Barcza from Vacuumschmelze for his kind support. Many thanks also to Eugene William from ENS Paris-Saclay, Marc Ardillier and Nicolas Mercadié from IUT de Cachan for their priceless technical help.

REFERENCES

[1] M. Gueltig, F. Wendler, H. Ossmer, M. Ohtsuka, H. Miki, T. Takagi, and M. Kohl, "High-Performance Thermomagnetic Generators Based on Heusler Alloy Films," *Advanced Energy Materials*, vol. 7, p. 1601879, Mar. 2017.

[2] V. K. Pecharsky and K. A. Gschneidner Jr, "Giant magnetocaloric effect in gd 5 (si 2 ge 2)," *Physical review letters*, vol. 78, no. 23, p. 4494, 1997.

[3] J. Lyubina, "Magnetocaloric materials for energy efficient cooling," *Journal of Physics D: Applied Physics*, vol. 50, no. 5, p. 053002, 2017.

[4] L. Brillouin and H. Iskenderian, "Thermomagnetic generator," *Electrical Communication*, vol. 25, p. 300, 1948.

[5] J. Chun, H.-C. Song, M.-G. Kang, H. B. Kang, R. A. Kishore, and S. Priya, "Thermo-Magneto-Electric Generator Arrays for Active Heat Recovery System," *Scientific Reports*, vol. 7, p. 41383, Feb. 2017.

[6] M. Ujihara, G. P. Carman, and D. G. Lee, "Thermal energy harvesting device using ferromagnetic materials," *Applied Physics Letters*, vol. 91, p. 093508, Aug. 2007.

[7] M. Gueltig, H. Ossmer, M. Ohtsuka, H. Miki, K. Tsuchiya, T. Takagi, and M. Kohl, "High frequency thermal energy harvesting using magnetic shape memory films," *Advanced Energy Materials*, vol. 4, 2014.

[8] A. Waske, D. Dzekan, K. Sellschopp, D. Berger, A. Stork, K. Nielsch, and S. Fähler, "Energy harvesting near room temperature using a thermomagnetic generator with a pretzel-like magnetic flux topology," *Nature Energy*, Dec. 2018.

[9] V. Priya, M. K. Rajendran, S. Kansal, G. Chowdary, and A. Dutta, "A human body heat driven high throughput thermal energy harvesting single stage regulator for wearable biomedical iot nodes," *IEEE Internet of Things Journal*, vol. 5, no. 6, pp. 4989–5001, 2018.

[10] S. Chalasani and J. M. Conrad, "A survey of energy harvesting sources for embedded systems," in *Southeastcon, 2008. IEEE*, pp. 442–447, IEEE, 2008.

[11] Q. Zhang and T. Zhang, "The refrigerant is also the pump," *Science*, vol. 357, no. 6356, pp. 1094–1095, 2017.

[12] L. Carlioz, *Générateur piézoélectrique à déclenchement thermo-magnétique*. PhD thesis, Institut National Polytechnique de Grenoble-INPG, 2009.

[13] M. Katter, V. Zellmann, G. W. Reppel, and K. Uestuener, "Magnetocaloric properties of $la(fe, co, si)_{13}$ bulk material prepared by powder metallurgy," *IEEE Transactions on Magnetics*, vol. 44, no. 11, pp. 3044–3047, 2008.

[14] A. Barcza, M. Katter, V. Zellmann, S. Russek, S. Jacobs, and C. Zimm, "Stability and magnetocaloric properties of sintered la (fe, mn, si) h alloys," *Magnetics, IEEE Transactions on*, vol. 47, no. 10, pp. 3391–3394, 2011.

[15] S. Ahmim, M. Almanza, A. Pasko, F. Mazaleyrat, and M. LoBue, "Thermal energy harvesting system based on magnetocaloric materials," *The European Physical Journal Applied Physics*, vol. 85, p. 10902, Jan. 2019.

[16] M. Almanza, A. Pasko, F. Mazaleyrat, and M. LoBue, "First- versus second-order magnetocaloric material for thermomagnetic energy conversion," *IEEE Transactions on Magnetics*, vol. 53, pp. 1–6, Nov 2017.

[17] F. Curzon and B. Ahlborn, "Efficiency of a carnot engine at maximum power output," *Am. J. Phys*, vol. 43, no. 1, pp. 22–24, 1975.

[18] C. R. H. Bahl and K. K. Nielsen, "The effect of demagnetization on the magnetocaloric properties of gadolinium," *Journal of Applied Physics*, vol. 105, no. 1, p. 013916, 2009.